

Article

Ozone Formation at a Suburban Site in the Pearl River Delta Region, China: Role of Biogenic Volatile Organic Compounds

Jun Wang^{1,2,3}, Yanli Zhang^{1,2,4,*}, Shaoxuan Xiao^{1,2,3} , Zhenfeng Wu^{1,2,3} and Xinming Wang^{1,2,3,4,*} 

¹ State Key Laboratory of Organic Geochemistry, Guangdong Key Laboratory of Environmental Protection and Resources Utilization, Guangzhou Institute of Geochemistry, Chinese Academy of Sciences, Guangzhou 510640, China

² CAS Center for Excellence in Deep Earth Science, Guangzhou 510640, China

³ University of Chinese Academy of Sciences, Beijing 100049, China

⁴ Center for Excellence in Regional Atmospheric Environment, Institute of Urban Environment, Chinese Academy of Sciences, Xiamen 361021, China

* Correspondence: zhang_y186@gig.ac.cn (Y.Z.); wangxm@gig.ac.cn (X.W.)

Abstract: Ozone (O₃) is becoming an increasingly concerning air quality problem in China, and previous O₃ control strategies focused primarily on reducing anthropogenic volatile organic compounds (AVOCs), while neglecting the role of biogenic VOCs (BVOCs) in O₃ formation. In this study, a field campaign was conducted at a suburban site in the Pearl River Delta region of China with high BVOC emissions from 29 August to 3 September 2020. An empirical kinetic modelling approach (EKMA) showed that VOC-limited was the dominant feature for O₃ formation at the site. The relative incremental reactivity (RIR) values calculated by the box model (AtChem2-MCM) revealed that isoprene, formaldehyde, methylglyoxal and acetaldehyde had the highest RIRs. Simulation results from the box model also showed that isoprene played a substantial role in the formation of secondary carbonyls, especially contributing 32–92% to the formaldehyde production rate. Box model simulations further showed that during the O₃ pollution period with high BVOC emissions, only near zero AVOC emissions could prevent O₃ if the levels of nitrogen oxides (NO_x) remained unchanged. The results suggest that the presence of high BVOC emissions can greatly impact efforts to control O₃ by reducing AVOCs, particularly in regions with relatively high NO_x levels (up to 51 ppbv in this study). In the long term, it may be essential to control NO_x and choose low BVOC-emitting tree species in urban planning to address this issue, particularly as BVOC emissions are projected to become a more significant source of reactive VOCs with enhanced control of AVOCs.

Keywords: ozone; biogenic volatile organic compounds; Master Chemical Mechanism (MCM); EKMA; RIR



Citation: Wang, J.; Zhang, Y.; Xiao, S.; Wu, Z.; Wang, X. Ozone Formation at a Suburban Site in the Pearl River Delta Region, China: Role of Biogenic Volatile Organic Compounds.

Atmosphere **2023**, *14*, 609. <https://doi.org/10.3390/atmos14040609>

Academic Editors: Duanyang Liu, Kai Qin and Honglei Wang

Received: 26 February 2023

Revised: 18 March 2023

Accepted: 20 March 2023

Published: 23 March 2023



Copyright: © 2023 by the authors. Licensee MDPI, Basel, Switzerland. This article is an open access article distributed under the terms and conditions of the Creative Commons Attribution (CC BY) license (<https://creativecommons.org/licenses/by/4.0/>).

1. Introduction

In the past three decades, severe ozone (O₃) pollution events have become more frequent, which has aroused public concern worldwide [1–4]. As a secondary product, surface O₃ is produced by a series of photochemical oxidation reactions between volatile organic compounds (VOCs) and nitrogen oxides (NO_x = NO + NO₂) in the presence of sunlight [5,6]. Elevated O₃ concentrations not only impact vegetation growth, crop yields and climate change [7–10], but also have severe adverse effects on human health [11,12].

Due to the nonlinear relationship between O₃ and its precursors, O₃ pollution is becoming an increasingly distinctive air pollution problem, especially in developing countries such as China [13–19]. O₃ formation is mostly in the VOC-limited regime in major urban agglomerations of China [20–25] and the transition regime or NO_x-limited regime typically occurs in suburban/rural areas [26–28]. Alkenes were found to be important O₃ precursors in the North China Plain (NCP) and Chengdu-Chongqing region [25,29,30], while aromatics and alkenes dominated O₃ formation in the Yangtze River Delta (YRD) region, such as

Shanghai and Hangzhou [31–34]. Studies in the suburban and rural sites of the Pearl River Delta (PRD) region have revealed that aromatics (such as xylenes and toluene) are the key precursors for O₃ formation [31,35,36], while both aromatics and alkenes contribute greatly to O₃ formation in downtown areas [30,37,38]. Nevertheless, recent studies revealed that biogenic VOCs (BVOCs) were among the more sensitive species to O₃ formation in terms of their incremental relative reactivity (RIR) in the PRD region in the tropical/subtropical southern China [39–41], or even in other areas of China [42,43]. The early studies in Atlanta, USA, with strong BVOC emissions showed that neglecting the impact of BVOCs on O₃ formation might overestimate the effectiveness of O₃ abatement strategies based on reducing anthropogenic VOCs, emphasizing that while controlling anthropogenic emissions of VOCs, attention should also be paid to the control of anthropogenic NO_x emissions [44,45]. As a matter of fact, BVOC emissions have been on the rise in China since 2010 [46]. Therefore, elucidating the role of BVOCs in O₃ formation is crucial for effectively regulating O₃ air pollution, especially in regions such as the PRD in south China, with relatively higher BVOC emissions [47].

The PRD region is one of the most developed urban agglomerations in China, where intensive anthropogenic VOC and NO_x emissions lead to O₃ air pollution, especially in the warm seasons [48,49]. In addition, the PRD region has a subtropical ocean monsoon climate characterized by abundant rainfall, high temperature and wide vegetation coverage. The vegetation type in this region is mainly subtropical evergreen broadleaf forest with high BVOC emission potentials [50–52]. BVOC emission inventories have shown that the annual average BVOC emission flux is much higher in the PRD region than in other parts of China [53,54]. Air quality modelling studies in the PRD region have indicated that BVOC emissions greatly impact the surface O₃ peak levels in summer and autumn, with a maximum increase of 20.0–34.0 ppbv [55–57], yet observation-based studies are needed to verify and deeply understand the effects of BVOCs at varied locations.

In this study, we conducted field measurements of O₃ and its precursors (VOCs and NO_x), as well as other trace gases, at a suburban site in the PRD region in 2020. The characteristics of BVOCs and their contributions to O₃ formation were investigated and compared with those of other VOC species. In addition, based on the box-model with the Master Chemical Mechanism (MCM v3.3.1), we explored to what extent reducing VOCs under the influence of BVOCs can alleviate O₃ air pollution.

2. Methodology

2.1. Site Description

The intensive field campaign was conducted from 29 August to 3 September 2020 at a site approximately 17 m above the ground on the roof top of a 6-storey building on the campus of Huadu Vocational and Technical School (23.39° N, 113.23° E; Figure S1), ~25 km away from the urban center in the north of Guangzhou. The vegetation coverage rate in Huadu District is 38.3% (data source: https://www.huadu.gov.cn/gkmlpt/content/8/8023/mpost_8023183.html (accessed on 20 February 2023)), and the plants around the site are eucalyptus, which has a high isoprene emission potential [58,59]. A state-controlled air quality monitoring station is located at this site. There are forest parks, residential buildings, traffic roads and scattered industrial blocks in the neighborhood (Figure S1).

2.2. Sample Collection and Chemical Analysis

Trace gases (i.e., NO-NO₂-NO_x, CO, SO₂ and O₃) and meteorological parameters (i.e., pressure, relative humidity (RH), temperature (T), solar radiation, wind speed and wind direction) were determined simultaneously during the campaign. The O₃ pollution days were defined as the days with a maximum daily 8-h average (MDA8) O₃ concentration exceeding the secondary standard limit of China's current National Ambient Air Quality Standard (NAAQS) of 160 µg m⁻³ (equivalent to 75 ppbv). According to the MDA8 O₃ levels, the whole observation period could be divided into a heavy O₃ pollution period (>95 ppbv; 29 August; P1), a light O₃ pollution period (75–85 ppbv; 1 September; P2), a mod-

erate O₃ pollution period (85–95 ppbv; 1–2 September; P3) and a non-O₃ pollution period (≤ 75 ppbv; 30–31 August; NP). Trace gases were monitored by online Thermo Scientific Environmental Instruments at the HD site, including the NO_x analyzer (Model 42i, Thermo Scientific Inc., Boston, Mass, USA), the gas filter correlation method CO analyzer (Model 48i, Thermo Scientific Inc., Boston, Mass, USA), the pulsed fluorescence SO₂ analyzer (Model 43i, Thermo Scientific Inc., Boston, Mass, USA) and the UV photometric O₃ analyzer (Model 49i, Thermo Scientific Inc., Boston, Mass, USA). Meteorological parameters were measured by an automatic weather station at the HD site. The solar radiation data were obtained from the monitoring data of the Guangzhou Meteorological Monitoring and Warning Center. The 3-h planetary boundary layer heights (PBLH) for the HD site were obtained from the Global Data Assimilation System (GDAS) (<https://ready.arl.noaa.gov/READYamet.php> (accessed on 12 November 2022)).

During the sampling period, 2-h average samples were consecutively taken at 6:00–8:00, 8:00–10:00, 10:00–12:00, 12:00–14:00, 14:00–16:00, 16:00–18:00, 18:00–20:00 and 20:00–22:00 local time (LT) every day. Cleaned and evacuated stainless-steel canisters were used to collect air samples with a model 910 canister sampler (Xonteck Inc., Fremont, CA, USA) to allow each canister to be filled within 120 min at a constant flow of 33.4 mL/min [41]. Ambient carbonyls were sampled simultaneously by drawing ambient air through 2,4-dinitrophenylhydrazine (DNPH)-coated sorbent cartridges. The nonmethane hydrocarbons (NMHCs) in the collected air samples were analyzed with an Agilent 5973N gas chromatography-mass selective detector/flame ionization detector (GC-MSD/FID, Agilent Technologies, USA). CH₄ in the air samples was also analyzed by a gas chromatography (Agilent 6890 GC, Agilent Technologies, Santa Clara, CA, USA) equipped with an FID (flame ionization detector) and a packed column (5A Molecular Sieve 60/80 mesh, 3 m × 1/8 inch). The detailed chemical analysis, quality control and quality assurance for NMHCs and CH₄ were given in our previous studies [60–64]. The carbonyls samples were analyzed by a high-performance liquid chromatography (HPLC) system (HP1200, Agilent Technologies, Santa Clara, CA, USA) and detected with an ultraviolet detector (the detecting wavelengths of monocarbonyl and dicarbonyl were 360 nm and 420 nm, respectively). The detailed laboratory analysis of carbonyls can be found elsewhere [65]. The method detection limits (MDLs) and average concentrations for the measured VOCs are listed in Table S1.

2.3. AtChem2-MCM Model

2.3.1. Model Description and Input

In this study, a zero-dimensional chemical box model coupled with Master Chemical Mechanism (version 3.3.1; <http://mcm.leeds.ac.uk> (accessed on 3 November 2022)) (AtChem2-MCM) was applied to investigate the relationships between O₃ and its precursors. This model provides near explicit gas-phase chemistry involving 6700 chemical species and 17,000 reactions [66–68]. The deposition processes of inorganic gases, oxygenated VOCs, PANs, peroxides and organic acids within the boundary layer were also considered in the model [31]. However, the model considered neither the heterogeneous reactions nor the transport process. Detailed descriptions about the parameters and model running can be found elsewhere [41,69].

The input data, including the NMHCs (alkanes, alkenes, alkynes, aromatics and BVOCs), carbonyls (formaldehyde, acetaldehyde, acetone, propionaldehyde, 2-butanone, benzaldehyde, glyoxal and methylglyoxal), CH₄, NO, NO₂, O₃, CO, SO₂ and meteorological parameters (temperature, pressure, relative humidity, boundary layer height and $j(\text{NO}_2)$) were averaged or interpolated with a time resolution of 1 h as the constraints of the model. The model was run at 00:00 local time (LT) as the initial time.

2.3.2. Model Performance

The index of agreement (IOA) with a value between 0 and 1, calculated by Equation (1) [70], is used to indicate the model performance. A higher value represents a better agreement between observation and simulation.

$$\text{IOA} = 1 - \frac{\sum_{i=1}^n (O_i - S_i)^2}{\sum_{i=1}^n (|O_i - \bar{O}| + |S_i - \bar{O}|)^2} \quad (1)$$

where O_i and S_i represent the observed and simulated values, respectively; \bar{O} represents the average of observations; and n is the number of samples. Figure S2 presents the comparison between the simulated model and the observed O_3 during the campaign, with an IOA value of 0.6. It is worth noting that during the study period, the daytime O_3 peak (15:00–18:00) appeared later than the solar radiation peak (12:00–13:00), and a small O_3 peak was also observed at night (up to 75.6 ppbv), indicating significant regional transport of O_3 at the HD site. This is the main reason affecting the performance of the box model considering only local production.

2.3.3. Relative Incremental Reactivity (RIR)

Relative incremental reactivity (RIR), which is defined as the ratio of the decrease in the O_3 production rate to the decrease in precursor concentrations without detailed knowledge of these emissions [71], has been widely applied in previous studies to indicate the sensitivity of O_3 formation to precursors [30,36,38,40,72,73]. With the AtChem2-MCM model, the RIR for a specific precursor X at site “S” is given by:

$$\text{RIR}^S(X) = \frac{[P_{O_3-NO}^S(X) - P_{O_3-NO}^S(X - \Delta X)] / P_{O_3-NO}^S(X)}{\Delta S(X) / S(X)} \quad (2)$$

$$P_{O_3-NO} = k_{HO_2+NO}[HO_2][NO] + k_{RO_2+NO}[RO_2][NO] - k_{O^1D+H_2O}[O^1D][H_2O] - k_{O_3+alkenes}[O_3][alkenes] - k_{O_3+OH}[O_3][OH] - k_{O_3+HO_2}[O_3][HO_2] - k_{NO_2+OH}[NO_2][OH] \quad (3)$$

where X represents the relevant precursor (VOC species, CO or NO); $S(X)$ is the observed concentrations of species X , which represents the combined flux of regional transport and the amounts emitted at the site; ΔX is the change in the concentration of X caused by a hypothetical change in $S(X)$ (20% $S(X)$ in this study); and $P_{O_3-NO}^S$ is defined as the O_3 formation potential from 07:00 to 19:00, which is the net amount of O_3 production and NO consumed (Equation (3)).

2.3.4. Empirical Kinetic Modelling Approach (EKMA)

The empirical kinetic modelling approach (EKMA) refers to a series of O_3 isopleths made by the photochemical reaction model, reflecting the nonlinear relationship between O_3 and its precursors to improve reduction strategies, as shown in Equation (4) [28,74]. EKMA judges its effect on the peak O_3 concentration by changing the initial concentration of O_3 precursors VOCs and NO_x to identify the response relationship between O_3 and its precursors. Generally, from the perspective of the feasibility of implementing control measures, only emission reduction control research is conducted on precursors emitted by anthropogenic sources, while VOCs emitted by biogenic sources remain at their original levels. In this study, the EKMA was based on MCM, and the measured 1-h averages of species except NO_x and VOCs during the whole campaign were used as the constraint conditions of the box model. The campaign-averaged concentrations of VOCs and NO_x from 7:00 to 19:00 were selected as the original concentrations (base case), and the concentrations of VOCs and NO_x were scaled under the base case. The daily maximum value of

O₃ generation was taken as the concentration after the reaction. The simulation period is from 6:00 to 20:00, where outdoor air quality has a greater impact on human activities.

$$P_{O_3} = f(\text{NO}_x \pm \Delta\text{NO}_x, \text{VOCs} \pm \Delta\text{VOCs}) \quad (4)$$

3. Results and Discussion

3.1. Overviews

3.1.1. Levels of Meteorological Parameters and Measured Species

Statistical descriptions about the levels of meteorological parameters and measured species at the HD site during the four periods are provided in Table 1, and their time series are presented in Figure 1. The daily averaged O₃ level in NP (50.6 ± 22.6 ppbv) was higher than that in P2 (43.3 ± 25.9 ppbv) or P3 (48.6 ± 35.0 ppbv), but lower than that in P1 (69.2 ± 33.1 ppbv), while the 1-h O₃ maximum value in NP (77.5 ppbv) was the lowest among that in P1 (127.0 ppbv), P2 (82.6 ppbv) and P3 (100.0 ppbv). MDA8 O₃ concentrations ranged from 63.4 ppbv (NP) to 98.6 ppbv (P1), which was comparable to those reported in polluted NCP and YRD regions [75–77]. The average concentrations of SO₂ and CO in NP were 1.8 ± 0.5 ppbv and 725.0 ± 96.8 ppbv, respectively, which were lower than those in the other three O₃ pollution periods. The levels of SO₂ and CO at the HD site were similar to those in some polluted suburban areas in the PRD region [31,40,78].

Table 1. Statistical descriptions about levels of meteorological parameters and measured species during the four periods (S.D.: standard deviation; BVOCs: biogenic VOCs; TVOCs: total VOCs).

	P1		P2		P3		NP	
	Average ± S.D.	Maximum						
Temperature (°C)	32.5 ± 2.13	35.2	31.5 ± 2.66	36.2	32.4 ± 2.43	35.9	31.2 ± 2.61	35.5
Solar radiation (W m ⁻²)	459 ± 330	886	544 ± 378	1016	511 ± 348	1018	434 ± 293	939
Relative humidity (%)	60.7 ± 8.91	78.0	66.4 ± 11.1	84.0	60.1 ± 11.0	80.0	67.3 ± 13.7	94.0
Wind speed (m s ⁻¹)	0.928 ± 0.351	1.90	0.900 ± 0.411	2.60	0.898 ± 0.283	1.40	1.01 ± 0.318	1.70
O ₃ (ppbv)	69.2 ± 33.1	127	43.3 ± 25.9	82.6	48.6 ± 35.0	100	50.6 ± 22.6	77.5
SO ₂ (ppbv)	2.06 ± 1.21	5.60	2.65 ± 1.50	5.60	1.76 ± 0.565	3.85	1.75 ± 0.473	3.50
CO (ppbv)	759 ± 80.5	913	779 ± 59.9	893	810 ± 87.0	1038	725 ± 96.8	879
NO (ppbv)	2.57 ± 1.82	7.47	1.71 ± 0.560	3.73	2.84 ± 3.82	22.4	2.05 ± 1.63	10.5
NO ₂ (ppbv)	21.1 ± 10.4	47.7	13.8 ± 7.56	32.6	18.6 ± 12.3	46.3	16.1 ± 12.3	48.7
Alkanes (ppbv)	18.6 ± 12.6	41.8	14.5 ± 11.4	31.2	17.0 ± 18.1	75.1	15.1 ± 13.2	54.8
Alkenes (ppbv)	1.42 ± 0.441	1.97	1.25 ± 0.474	1.96	1.43 ± 0.624	2.92	1.39 ± 0.605	3.09
Aromatics (ppbv)	3.31 ± 2.48	7.42	1.66 ± 1.88	5.97	2.45 ± 2.58	10.6	3.45 ± 3.37	11.9
Alkynes (ppbv)	1.08 ± 0.475	1.87	0.868 ± 0.228	1.07	1.07 ± 0.480	1.94	1.09 ± 0.444	1.74
Carbonyls (ppbv)	18.8 ± 4.57	25.3	11.0 ± 0.773	11.8	15.6 ± 2.17	19.6	16.0 ± 2.86	22.3
BVOCs (ppbv)	1.24 ± 1.90	4.70	2.11 ± 2.12	5.55	2.14 ± 1.76	5.39	1.68 ± 1.41	4.41
TVOCs (ppbv)	44.5 ± 16.7	76.2	25.9 ± 14.1	52.0	39.7 ± 18.8	96.5	38.7 ± 17.6	84.1

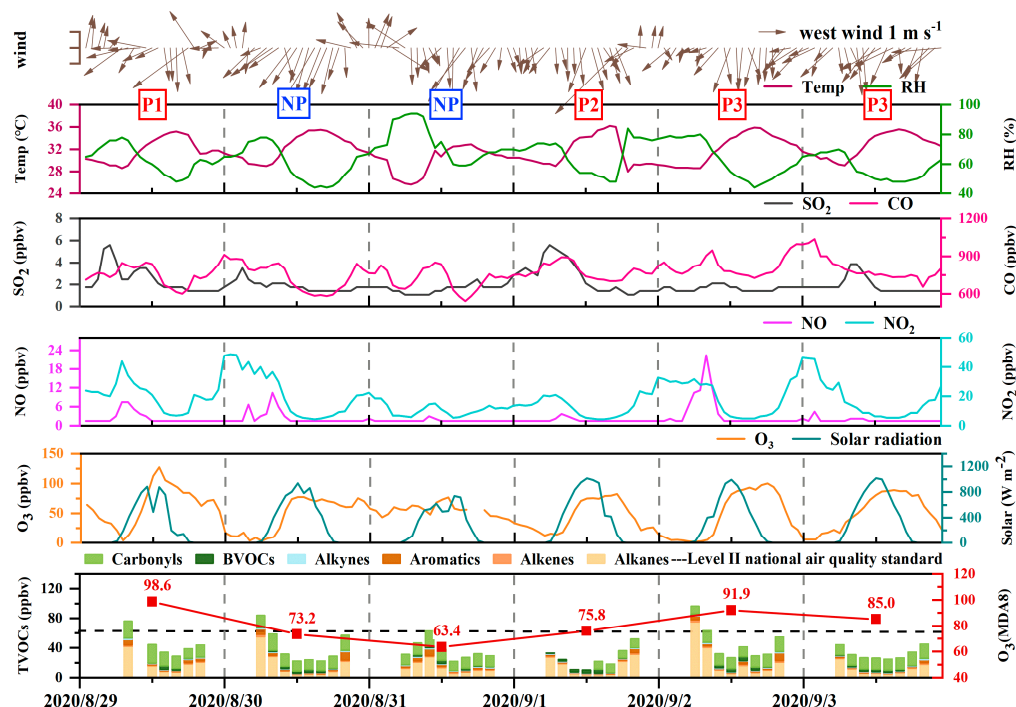


Figure 1. Time series of meteorological parameters and measured species observed at HD during three O₃ pollution periods (P1, P2, P3; 29 August and 1–3 September 2020) and one non-O₃ pollution period (NP; 30–31 August 2020). Due to instrument failure, the carbonyl data from 6:00–12:00 on 1 September are missing. Other data gaps were mainly due to instrument maintenance and calibration. Temp: temperature; RH: relative humidity; BVOCs: biogenic VOCs; MDA8: maximum daily 8-h average.

As for the O₃ precursors, the average NO_x concentration was approximately 20 ppbv (up to 51 ppbv), which was higher than in some polluted suburban areas and even a few urban areas [38,40,73,79], and lower than most urban areas [41,73,80,81]. Due to the morning peak, the peak of NO usually occurred around 8:00 and could reach up to 22.4 ppbv, while the NO₂ concentration level was very high during 21:00–9:00, up to 48.7 ppbv, which might be related to the higher NO_x emissions from diesel vehicles at night. The average TVOCs concentration (~37.2 ppbv) was between the values previously reported in the PRD region, ranging from 21.1 to 73.8 ppbv [36,41,49,82,83]. Both NO_x and total VOCs (TVOCs) (including 62 NMHCs and 8 carbonyls) showed higher mixing ratios in P1 (23.6 ± 11.6 ppbv and 44.5 ± 16.7 ppbv, respectively) compared with the other three periods (Table 1). A comparison between P3 and NP revealed that TVOCs were comparable in P3 and NP, while NO_x was 18% higher in P3 than in NP (Table 1). The average concentrations of NO_x and TVOCs in P2 were 15.5 ± 7.7 ppbv and 25.9 ± 14.1 ppbv, respectively, which were not only lower than those in P1 or P3, but even lower than those in NP. However, the proportion of active VOCs (BVOCs and carbonyls) in P2 (51%) was much higher than that in P1 (45%), P3 (45%) or NP (46%), especially the BVOCs concentration, which was up to 5.6 ppbv. The mean temperature (31.2 ± 2.6 °C) and solar radiation (434 ± 293 W m⁻²) in NP were lower than that in P1 (32.5 ± 2.1 °C, 459 ± 330 W m⁻²), P2 (31.5 ± 2.7 °C, 544 ± 378 W m⁻²) and P3 (32.4 ± 2.43 °C, 511 ± 348 W m⁻²), while the mean relative humidity (67.3 ± 13.7%) was higher than that in P1 (60.7 ± 8.9%), P2 (66.4 ± 11.1%) and P3 (60.1 ± 11.0%). In all four periods, the mean wind speeds were similar (~1 m s⁻¹). The ratio of toluene to benzene (T/B) has been widely used to represent the source contribution of aromatic solvents, with a value greater than 3 indicating the presence of solvent-related sources [84–86]. Although T/B ratios averaged 11 in NP, which were over 20% higher than that of 7 in P1, 9 in P2 or 6 in P3 (Figure S3), the adverse meteorological conditions (the weakest solar radiation, the lowest temperature and the highest relative humidity) in NP offset the impact of aromatic

solvents on O₃ formation. Therefore, meteorological factors might be the main reason affecting whether the MDA8 O₃ concentration exceeded the guideline standard (75 ppbv) in this O₃ pollution process.

3.1.2. Diurnal Variation

Figure 2 presents the average diurnal variations in meteorological parameters and major trace gases at HD during the four periods. These diurnal variations reflected the interplay of primary emissions, atmospheric photochemical processes, and meteorological conditions. With the gradual increase in solar radiation, the O₃ concentration began to increase in the early morning (approximately 06:00). Different from previous studies showing a unimodal O₃ diurnal variation (reaching a peak at approximately midday and then decreasing) in some urban areas [21,25,87,88], the O₃ concentrations in this study exhibited a broadened peak in the afternoon (12:00–18:00 LT) at the HD site due to the influence of regional transport [89]. Compared with the three O₃ pollution periods, the daytime O₃ levels in NP were significantly lower, accompanied by a lower temperature, weaker solar radiation and higher humidity. However, at night and in the early morning (0:00–9:00 and 21:00–24:00), the O₃ concentrations in NP were higher than that in P2 and P3, which might be due to regional transport (wind speeds up to ~2 m s⁻¹).

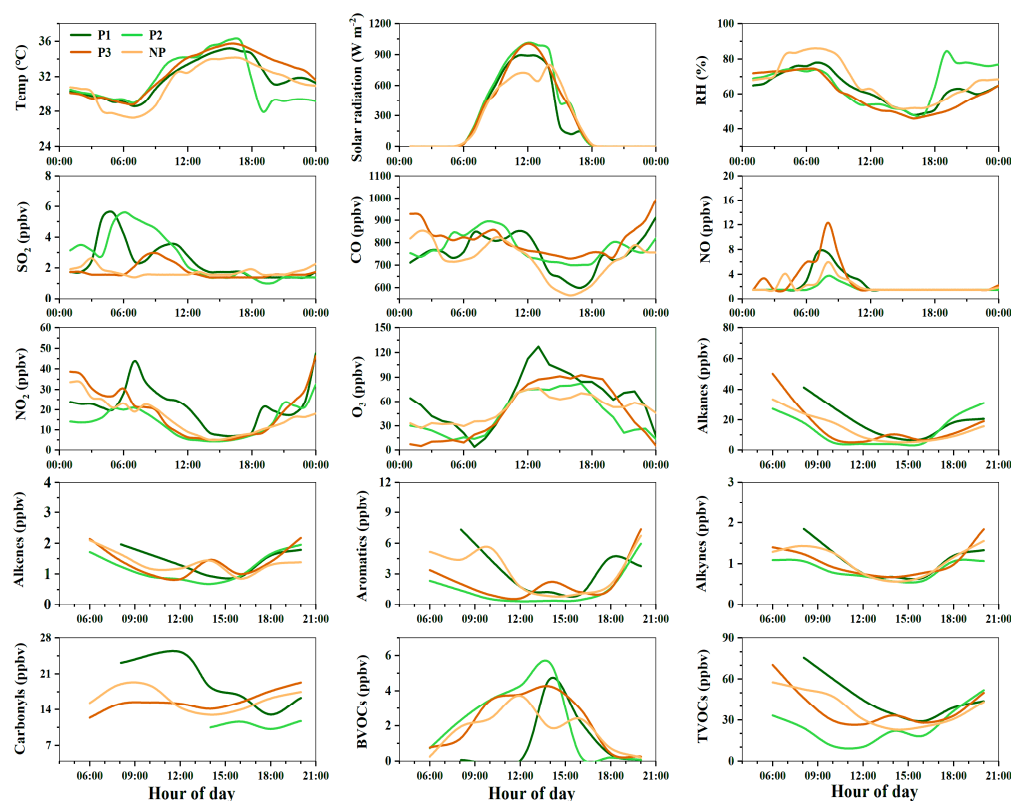


Figure 2. Diurnal variations in meteorological parameters and major trace gases during the four periods. It should be noted that only daytime (6:00–20:00 LT) data were measured.

Diurnal variations in NO, NO₂ and CO all showed peaks in the morning rush hour at approximately 9:00, with the lowest concentrations at approximately 15:00 in the afternoon, and NO₂ and CO also showed high concentrations during the evening. The diurnal variations in the VOC groups (including alkanes, alkenes, aromatics, alkynes and carbonyls) showed variations similar to those of CO and NO_x, which might be related to significant primary emissions (e.g., vehicle exhaust), photochemical reaction consumption and boundary layer uplift at noon. In comparison, the diurnal variation in BVOCs was different from that of other VOCs, with the maximum value appearing at 12:00–15:00, corresponding

to the maximum temperature value, and the maximum value in NP was smaller than in the other three O₃ pollution periods. Previous studies have shown that high temperature could promote BVOC emissions [90–92]. In addition, the average levels of carbonyls in all periods were higher in the morning and evening and peaked at noon (approximately 12:00), reflecting the combined impact of primary emissions and secondary formation.

3.2. O₃-Precursor Relationships

3.2.1. O₃-VOCs-NO_x Sensitivity

The change of NO_x and VOCs will influence the O₃ production, and this O₃-VOCs-NO_x sensitivity can be reflected by the O₃ isopleth diagram. The base case model input data can be found in Section 2.3.4. Based on the base case, VOCs and NO_x were scaled to obtain 77 model scenarios (11 NO_x × 7 VOCs), and the maximum O₃ under each scenario was selected to plot the O₃ isopleth, as shown in Figure 3a. The grid line divides the diagram into two parts, namely VOC-limited (upper) and NO_x-limited (lower) regimes. It was clear that the whole sampling period was above the grid line, except 31 August, which was slightly below the grid line, indicating that VOC-limited was the dominant feature for O₃ production at this site. This result was consistent with previous studies in the PRD region [30,83,93,94], indicating that reducing VOCs could depress O₃ formation.

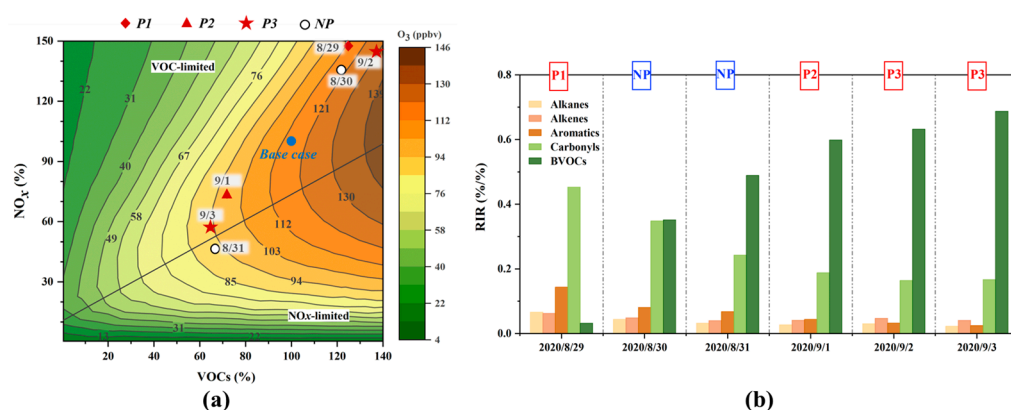


Figure 3. The O₃-VOCs-NO_x sensitivity study for the HD site. (a) The O₃ isopleth diagram versus NO_x and VOCs using EKMA (the horizontal and vertical axes represent the percentage of original mixing ratios of VOCs and NO_x: the percentage change of VOCs from 0.5% to 140% and the percentage change of NO_x from 0.5% to 150%. The isopleths give the peak O₃ in the unit of ppbv.); (b) RIR (relative incremental reactivity) values of major VOC groups during the four periods, i.e., alkanes, alkenes, aromatics, carbonyls and BVOCs.

Figure 3b shows the model-calculated RIR values of the VOC groups including alkanes, alkenes, aromatics, carbonyls and BVOCs. In all the VOC groups, except for carbonyls with the highest RIR value in P1, BVOCs had the highest RIRs (0.55 ± 0.13) in the other three periods, which was similar to the results previously reported in urban Guangzhou [41] and suburban Wuhan [95] on O₃ episode days. Carbonyls (0.22 ± 0.08) showed a lower RIR value than BVOCs, but the level was also much higher than those of aromatics (0.05 ± 0.02), alkenes (0.04 ± 0.01) and alkanes (0.03 ± 0.01) during P2, P3 and NP. Similarly, it was also found that the pattern of diurnal variations in the RIRs of VOC groups in P1 was completely different from the patterns of the other three periods (Figure 4). In P1, the RIRs of carbonyls were significantly higher than those in the other three periods, with the maximum occurring at approximately 9:00 and the minimum occurring at approximately 18:00, which was similar to the diurnal variations of their concentrations (Figure 2). The RIRs of BVOCs showed a trend of being higher in the morning and evening and lower around noon in P1 due to the lower concentrations of BVOCs in the 9:00–13:00 period (<1 ppbv), contrary to the other three periods. Our results demonstrate that the dominant

roles of BVOCs in O_3 formation in the suburban area of the PRD region were associated with higher BVOC emissions.

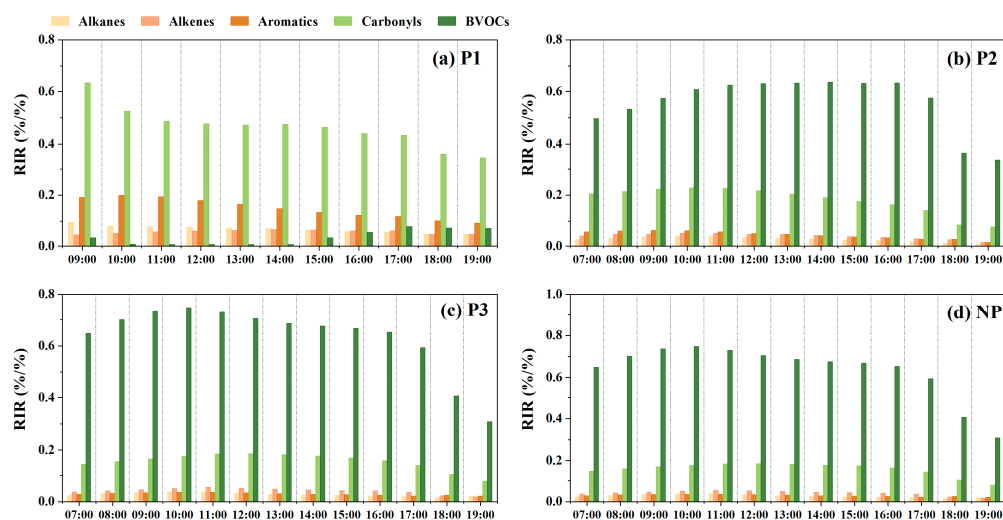


Figure 4. Average diurnal variations of RIR values of VOC groups in (a) P1, (b) P2, (c) P3 and (d) NP.

3.2.2. Relative Importance of VOCs in O_3 Formation

The RIR values of each VOC species were further calculated, and the top 5 VOC species with average RIR values were selected during the four periods, as shown in Figure 5. The daily top 10 VOC species with RIR values can be found in Table S2. It was found that formaldehyde was the most sensitive to O_3 formation in P1, while isoprene was the most sensitive to O_3 formation in the other three periods. The RIR values of isoprene, formaldehyde, methylglyoxal and acetaldehyde ranked in the top 5 in all four study periods. The difference was that the RIRs of m/p-xylene also ranked in the top 5 in P1 and NP, while those of α -pinene ranked in the top 5 in P2 and P3. It was found that isoprene was also ranked first by RIRs at a suburban site in Hong Kong and a rural site in Zhuhai, Guangdong [40]. Isoprene was also found to be most sensitive to O_3 formation in central and southwestern China, which has high forest coverage [42,43].

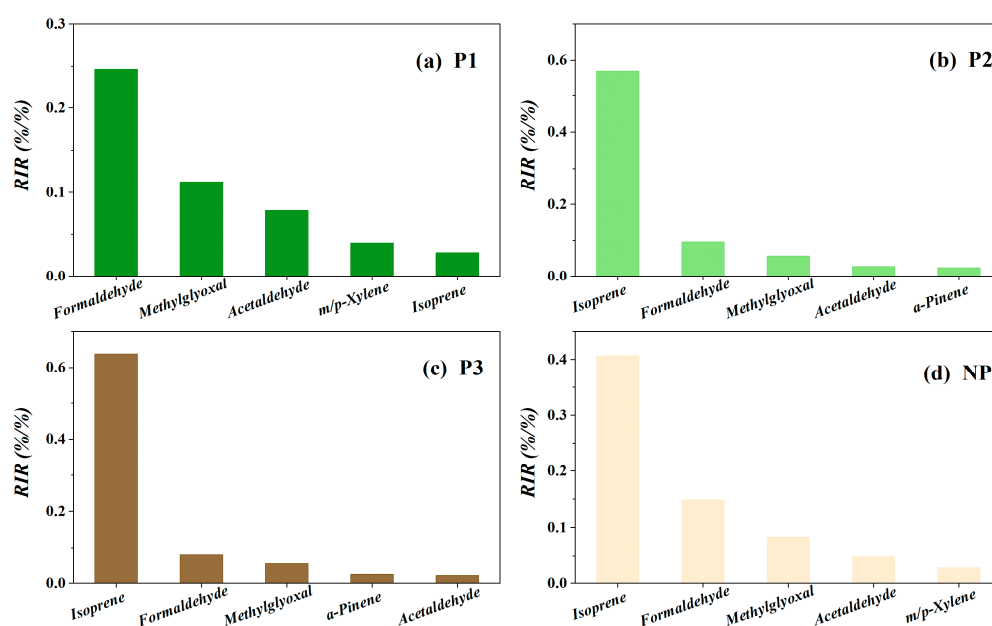


Figure 5. Average RIR values of the top 5 VOC species for O_3 at HD in (a) P1, (b) P2, (c) P3 and (d) NP.

In this study, isoprene was also an important precursor of carbonyls, especially the contribution to formaldehyde, methylglyoxal and glyoxal, which ranked first (Figure S4), and these carbonyls were more sensitive to O₃ formation, which meant that isoprene was the most sensitive species to O₃ formation. Figure 6 shows the model-calculated formaldehyde production rate from the degradation of VOC species during the four periods. In P1, P2, P3 and NP, the contribution of isoprene to the total formaldehyde production rate far exceeded that of other VOC species, with contribution rates of 32%, 92%, 92% and 78%, respectively. The contribution of isoprene to the formaldehyde production rate was different in the fourth period, which was mainly related to the isoprene concentration, and the higher the concentration, the greater the contribution. It is worth noting that the factors affecting the difference of BVOC levels in the four periods are different. BVOC concentrations in P1 were very low (<1 ppbv) from 7:00 to 13:00, but more than 1 ppbv after 13:00 (Figure 2). The change of BVOC concentrations in P1 corresponded to the change of wind direction, that is, from easterly wind (7:00–13:00) to northerly wind (14:00–17:00), while in other periods, northerly wind dominated during the day (Figure 1), indicating that the change of wind direction might affect the contribution of emission sources to the VOCs' concentrations. The contribution of isoprene to the formaldehyde production rate in NP was less than that in P2 and P3, mainly related to the lower temperature in NP (31.2 ± 2.6 °C) than in P2 (31.5 ± 2.7 °C) and P3 (32.4 ± 2.43 °C), and previous studies have shown that a high temperature could promote BVOC emissions [90–92]. In addition to isoprene, aromatics (e.g., toluene, xylenes and ethylbenzene) and alkenes (e.g., propene, trans-2-butene and cis-2-butene) were also important precursors of carbonyls. Moreover, in previous studies in some areas of the PRD, aromatics and alkenes were still the most important O₃ precursors [35,37,41,81,96]. In the case of difficult control of isoprene, the effectiveness of controlling anthropogenic VOC (AVOC) emissions to alleviate O₃ pollution is discussed further below.

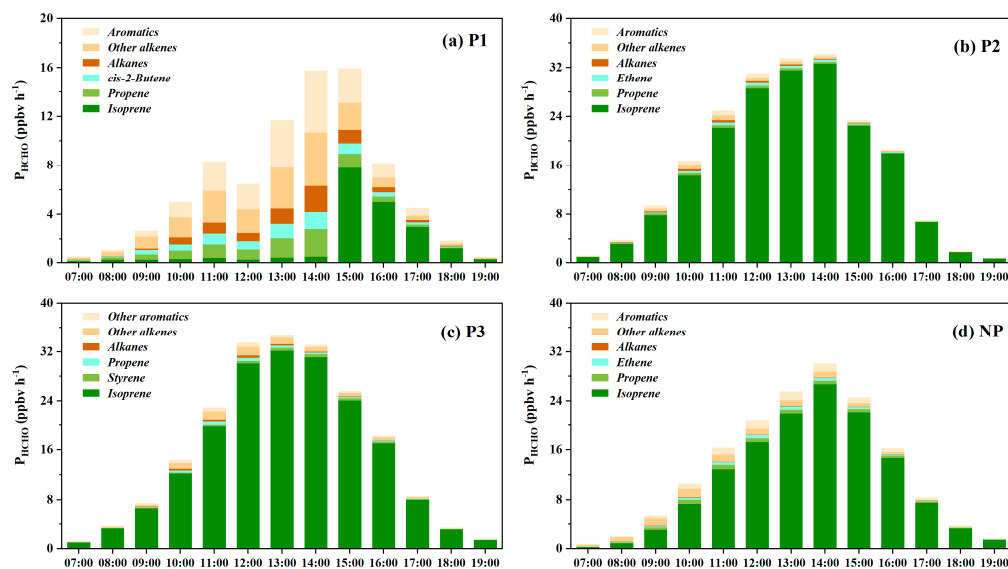


Figure 6. The model-calculated formaldehyde production rate from the degradation of VOC species in (a) P1, (b) P2, (c) P3 and (d) NP.

3.3. AVOCs Control Strategies under the Influence of High BVOC Levels

From the discussions and results above, it can be seen that the sensitivity of BVOCs to O₃ formation is dominant, but the emission of BVOCs is difficult to effectively control in the short-term. Therefore, more attention should be paid to controlling AVOC emissions, especially in areas where O₃ formation is VOC-limited but BVOC levels are high. AVOCs are emitted from various sources, among which alkanes mainly come from gasoline-related emission sources (e.g., on-road mobile source and fuel oil storage and transportation),

alkenes from combustion sources (e.g., mobile source and biomass combustion), aromatics from industrial-related emission sources, and primary carbonyls mainly come from cooking processes [85,97–100]. Then, under the existing atmospheric conditions, it is a question of to what extent to control the AVOCs to effectively alleviate O₃ pollution.

Considering that formaldehyde was the most sensitive to O₃ formation among the carbonyls and mainly came from the secondary oxidation process of isoprene, we designed a series of AVOC concentration reduction schemes while keeping the concentrations of NO_x, BVOCs and formaldehyde unchanged. The results are shown in Figure 7. There were four O₃ pollution days during the whole observation period, August 29 (P1), 1 September (P2) and 2–3 September (P3), with the maximum concentration of MDA8 O₃ concentrations on 29 August being approximately 99 ppbv. It was found that with the decreasing percentage of AVOC concentrations gradually increasing from 0 to 100%, the MDA8 O₃ concentrations in P1 rapidly decreased from 99 ppbv to 41 ppbv by ~59%. However, when the AVOCs levels were reduced by 100%, the MDA8 O₃ concentrations in P2 and P3 decreased by only ~20%, and for each day, the MDA8 O₃ concentrations decreased from 76 ppbv to 59 ppbv on 1 September, from 92 ppbv to 74 ppbv on 2 September, and from 85 ppbv to 70 ppbv on 3 September. For P2, when the MDA8 O₃ concentration only slightly exceeded the guideline standard (75 ppbv), it only needed to reduce the AVOC levels by 10% to make the MDA8 O₃ concentration meet the standard. For P1 and P3 with serious O₃ pollution, cutting the AVOC levels by 50% could make the MDA8 O₃ concentration meet the standard in P1 with low BVOC emissions, while in P3 with high BVOC emissions, reducing the AVOC concentrations to zero could eliminate the occurrence of O₃ pollution in the region, suggesting that the presence of high BVOC emissions can greatly impact efforts to control O₃ by reducing AVOCs, particularly in regions with relatively high NO_x levels.

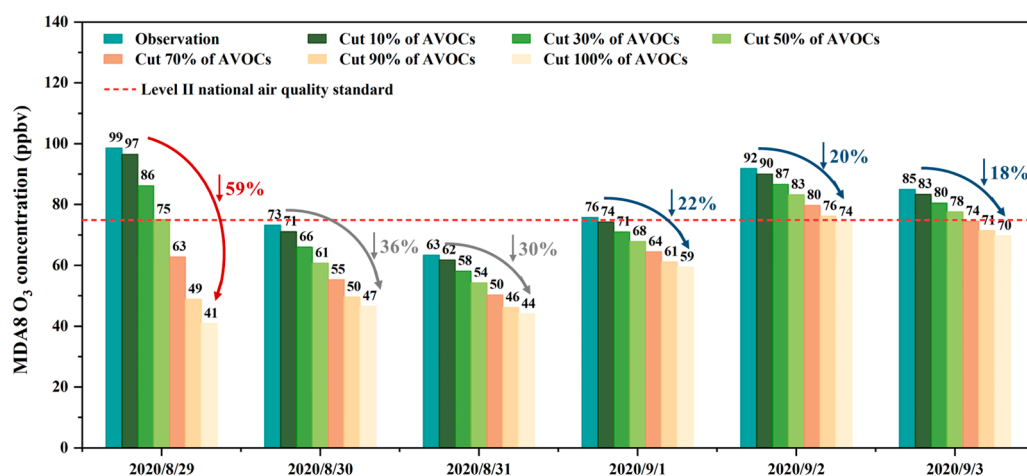


Figure 7. MDA8 O₃ concentrations during the whole campaign and under the condition of reducing different proportions of AVOCs.

4. Conclusions

In this study, O₃ and its precursors were measured at a suburban site in South China with large BVOC emissions during four periods, including a heavy O₃ pollution period (P1), a light O₃ pollution period (P2), a moderate O₃ pollution period (P3) and a non-O₃ pollution period (NP), and the AtChem2-MCM box model was applied to investigate the O₃-precursor relationships. Although the average concentrations of NO_x and TVOCs in NP were lower than those in P1 and P3, both were higher than those in P2, and the proportion of active VOCs in NP (46%) was slightly higher than that in P1 (45%) and P3 (45%), but lower than that in P2 (51%). The T/B ratios in NP (~11) were also over 20% higher than that during the O₃ pollution period (P1, P2 or P3), but the adverse meteorological conditions (the weakest solar radiation, the lowest temperature and the highest relative humidity) in NP offset the impact of aromatic solvents on O₃ formation, demonstrating meteorological

factors might be the main reason affecting whether the MDA8 O₃ concentration exceeded the guideline standard (75 ppbv).

The box model simulations revealed that VOC-limited was the dominant feature for O₃ formation during this whole sampling period, implying that controlling VOCs was more effective than NO_x in mitigating O₃ formation. BVOCs had the highest relative incremental reactivity (RIR) values in P2, P3 or NP, while carbonyls had the highest RIR value in P1. The pattern of diurnal variations in the RIRs of the VOC groups in P1 was also completely different from the patterns of the other three periods, especially for BVOCs, which was mainly related to their concentration levels. Isoprene, formaldehyde, methylglyoxal and acetaldehyde had the highest RIRs in all four study periods. Isoprene also played a substantial role in the formation of secondary carbonyls, especially contributing 32–92% to the formaldehyde production rate. In addition to isoprene, aromatics and alkenes were also important precursors that dominated the secondary formation of carbonyls, indicating that controlling them was the key to controlling O₃ pollution. However, the emission of BVOCs is difficult to control effectively in the short term, and more attention should be paid to controlling AVOC emissions. Box model simulations showed that during the O₃ pollution period with high BVOC emissions, only near zero AVOC emissions could prevent O₃ if the levels of NO_x remained unchanged. The results suggest that the presence of high BVOC emissions can greatly impact efforts to control O₃ by reducing AVOCs, particularly in regions with relatively high NO_x levels (up to 51 ppbv in this study).

Supplementary Materials: The following supporting information can be downloaded at: <https://www.mdpi.com/article/10.3390/atmos14040609/s1>, Figure S1: Location of the HD sampling site; Figure S2: Simulated and observed O₃ during O₃ pollution (O₃ episode days) and clean (non-O₃ episode days) days; Figure S3: Scatter plots of toluene to benzene during four periods; Figure S4: Average RIR values of the top 10 VOC species for (a) formaldehyde, (b) acetaldehyde, (c) glyoxal and (d) methylglyoxal during the whole campaign; Table S1: The average mixing ratios and 95% confidence intervals (95% C.I.) of TVOCs (pptv) measured during the four periods; Table S2: Top 10 VOC species with RIR values.

Author Contributions: Conceptualization, X.W.; methodology, J.W., Y.Z., S.X. and Z.W.; validation, X.W.; formal analysis, J.W.; investigation, J.W.; data curation, X.W. and Y.Z.; writing—original draft preparation, J.W.; writing—review and editing, X.W. and Y.Z.; supervision, X.W. and Y.Z.; funding acquisition, X.W. and Y.Z. All authors have read and agreed to the published version of the manuscript.

Funding: This research was funded by the National Natural Science Foundation of China (42022023), the Chinese Academy of Sciences (XDA23020301 and XDA23010303), the Youth Innovation Promotion Association of the Chinese Academy of Sciences (Y2021096), the Hong Kong Theme-base project (T24-504/17-N), the Department of Science and Technology of Guangdong Province (2020B1212060053 and 2019B121205006) and the Guangzhou Municipal Science and Technology Bureau (202206010057).

Institutional Review Board Statement: Not applicable.

Informed Consent Statement: Not applicable.

Data Availability Statement: Data are available upon request from the corresponding author (wangxm@gig.ac.cn).

Acknowledgments: The authors acknowledge the support of the Guangzhou Ecological and Environmental Monitoring Center of Guangdong Province.

Conflicts of Interest: The authors declare no conflict of interest.

References

1. Oltmans, S.J.; Johnson, B.J.; Harris, J.M.; Thompson, A.M.; Liu, H.Y.; Chan, C.Y.; Vomel, H.; Fujimoto, T.; Brackett, V.G.; Chang, W.L.; et al. Tropospheric ozone over the North Pacific from ozonesonde observations. *J. Geophys. Res. Atmos.* **2004**, *109*, D15S01. [[CrossRef](#)]
2. Monks, P.S.; Archibald, A.T.; Colette, A.; Cooper, O.; Coyle, M.; Derwent, R.; Fowler, D.; Granier, C.; Law, K.S.; Mills, G.E.; et al. Tropospheric ozone and its precursors from the urban to the global scale from air quality to short-lived climate forcer. *Atmos. Chem. Phys.* **2015**, *15*, 8889–8973. [[CrossRef](#)]
3. Li, K.; Jacob, D.J.; Liao, H.; Zhu, J.; Shah, V.; Shen, L.; Bates, K.H.; Zhang, Q.; Zhai, S.X. A two-pollutant strategy for improving ozone and particulate air quality in China. *Nat. Geosci.* **2019**, *12*, 906–910. [[CrossRef](#)]
4. Benish, S.E.; He, H.; Ren, X.R.; Roberts, S.J.; Salawitch, R.J.; Li, Z.Q.; Wang, F.; Wang, Y.Y.; Zhang, F.; Shao, M.; et al. Measurement report: Aircraft observations of ozone, nitrogen oxides, and volatile organic compounds over Hebei Province, China. *Atmos. Chem. Phys.* **2020**, *20*, 14523–14545. [[CrossRef](#)]
5. Carter, W.P.L.; Pierce, J.A.; Luo, D.M.; Malkina, I.L. Environmental chamber study of maximum incremental reactivities of volatile organic-compounds. *Atmos. Environ.* **1995**, *29*, 2499–2511. [[CrossRef](#)]
6. Jenkin, M.E.; Clemitshaw, K.C. Ozone and other secondary photochemical pollutants: Chemical processes governing their formation in the planetary boundary layer. *Atmos. Environ.* **2000**, *34*, 2499–2527. [[CrossRef](#)]
7. Unger, N.; Bond, T.C.; Wang, J.S.; Koch, D.M.; Menon, S.; Shindell, D.T.; Bauer, S. Attribution of climate forcing to economic sectors. *Proc. Natl. Acad. Sci. USA* **2010**, *107*, 3382–3387. [[CrossRef](#)]
8. Wilkinson, S.; Mills, G.; Illidge, R.; Davies, W.J. How is ozone pollution reducing our food supply? *J. Exp. Bot.* **2012**, *63*, 527–536. [[CrossRef](#)]
9. Yue, X.; Unger, N.; Harper, K.; Xia, X.G.; Liao, H.; Zhu, T.; Xiao, J.F.; Feng, Z.Z.; Li, J. Ozone and haze pollution weakens net primary productivity in China. *Atmos. Chem. Phys.* **2017**, *17*, 6073–6089. [[CrossRef](#)]
10. Mills, G.; Sharps, K.; Simpson, D.; Pleijel, H.; Broberg, M.; Uddling, J.; Jaramillo, F.; Davies, W.J.; Dentener, F.; Van den Berg, M.; et al. Ozone pollution will compromise efforts to increase global wheat production. *Glob. Chang. Biol.* **2018**, *24*, 3560–3574. [[CrossRef](#)]
11. Lelieveld, J.; Evans, J.S.; Fnais, M.; Giannadaki, D.; Pozzer, A. The contribution of outdoor air pollution sources to premature mortality on a global scale. *Nature* **2015**, *525*, 367–371. [[CrossRef](#)] [[PubMed](#)]
12. Malley, C.S.; Henze, D.K.; Kuylenstierna, J.C.I.; Vallack, H.W.; Davila, Y.; Anenberg, S.C.; Turner, M.C.; Ashmore, M.R. Updated global estimates of respiratory mortality in adults ≥ 30 years of age attributable to long-term ozone exposure. *Environ. Health Perspect.* **2017**, *125*, 087021. [[CrossRef](#)]
13. Zhang, X.Y.; Wang, Y.Q.; Niu, T.; Zhang, X.C.; Gong, S.L.; Zhang, Y.M.; Sun, J.Y. Atmospheric aerosol compositions in China: Spatial/temporal variability, chemical signature, regional haze distribution and comparisons with global aerosols. *Atmos. Chem. Phys.* **2012**, *12*, 779–799. [[CrossRef](#)]
14. Guo, S.; Hu, M.; Zamora, M.L.; Peng, J.F.; Shang, D.J.; Zheng, J.; Du, Z.F.; Wu, Z.; Shao, M.; Zeng, L.M.; et al. Elucidating severe urban haze formation in China. *Proc. Natl. Acad. Sci. USA* **2014**, *111*, 17373–17378. [[CrossRef](#)]
15. Hu, J.L.; Chen, J.J.; Ying, Q.; Zhang, H.L. One-year simulation of ozone and particulate matter in China using WRF/CMAQ modeling system. *Atmos. Chem. Phys.* **2016**, *16*, 10333–10350. [[CrossRef](#)]
16. Wang, T.; Xue, L.; Brimblecombe, P.; Lam, Y.F.; Li, L.; Zhang, L. Ozone pollution in China: A review of concentrations, meteorological influences, chemical precursors, and effects. *Sci. Total Environ.* **2017**, *575*, 1582–1596. [[CrossRef](#)] [[PubMed](#)]
17. Lu, X.; Hong, J.Y.; Zhang, L.; Cooper, O.R.; Schultz, M.G.; Xu, X.B.; Wang, T.; Gao, M.; Zhao, Y.H.; Zhang, Y.H. Severe surface ozone pollution in China: A global perspective. *Environ. Sci. Technol. Lett.* **2018**, *5*, 487–494. [[CrossRef](#)]
18. Li, K.; Jacob, D.J.; Liao, H.; Shen, L.; Zhang, Q.; Bates, K.H. Anthropogenic drivers of 2013–2017 trends in summer surface ozone in China. *Proc. Natl. Acad. Sci. USA* **2019**, *116*, 422–427. [[CrossRef](#)]
19. Li, K.; Jacob, D.J.; Shen, L.; Lu, X.; De Smedt, I.; Liao, H. Increases in surface ozone pollution in China from 2013 to 2019: Anthropogenic and meteorological influences. *Atmos. Chem. Phys.* **2020**, *20*, 11423–11433. [[CrossRef](#)]
20. Shao, M.; Zhang, Y.H.; Zeng, L.M.; Tang, X.Y.; Zhang, J.; Zhong, L.J.; Wang, B.G. Ground-level ozone in the Pearl River Delta and the roles of VOC and NO_x in its production. *J. Environ. Manag.* **2009**, *90*, 512–518. [[CrossRef](#)]
21. An, J.L.; Zou, J.N.; Wang, J.X.; Lin, X.; Zhu, B. Differences in ozone photochemical characteristics between the megacity Nanjing and its suburban surroundings, Yangtze River Delta, China. *Environ. Sci. Pollut. Res.* **2015**, *22*, 19607–19617. [[CrossRef](#)] [[PubMed](#)]
22. Ou, J.M.; Yuan, Z.B.; Zheng, J.Y.; Huang, Z.J.; Shao, M.; Li, Z.K.; Huang, X.B.; Guo, H.; Louie, P.K.K. Ambient ozone control in a photochemically active region: Short term despiking or long-term attainment? *Environ. Sci. Technol.* **2016**, *50*, 5720–5728. [[CrossRef](#)] [[PubMed](#)]
23. Han, X.; Zhu, L.Y.; Wang, S.L.; Meng, X.Y.; Zhang, M.G.; Hu, J. Modeling study of impacts on surface ozone of regional transport and emissions reductions over North China Plain in summer 2015. *Atmos. Chem. Phys.* **2018**, *18*, 12207–12221. [[CrossRef](#)]
24. Xing, J.; Ding, D.; Wang, S.X.; Zhao, B.; Jang, C.; Wu, W.J.; Zhang, F.F.; Zhu, Y.; Hao, J.M. Quantification of the enhanced effectiveness of NO_x control from simultaneous reductions of VOC and NH₃ for reducing air pollution in the Beijing-Tianjin-Hebei region, China. *Atmos. Chem. Phys.* **2018**, *18*, 7799–7814. [[CrossRef](#)]

25. Tan, Z.F.; Lu, K.D.; Jiang, M.Q.; Su, R.; Dong, H.B.; Zeng, L.M.; Xie, S.D.; Tan, Q.W.; Zhang, Y.H. Exploring ozone pollution in Chengdu, southwestern China: A case study from radical chemistry to O₃-VOC-NO_x sensitivity. *Sci. Total Environ.* **2018**, *636*, 775–786. [[CrossRef](#)]
26. Xu, J.; Zhang, Y.; Fu, J.S.; Zheng, S.; Wang, W. Process analysis of typical summertime ozone episodes over the Beijing area. *Sci. Total Environ.* **2008**, *399*, 147–157. [[CrossRef](#)]
27. Pan, X.; Kanaya, Y.; Tanimoto, H.; Inomata, S.; Wang, Z.; Kudo, S.; Uno, I. Examining the major contributors of ozone pollution in a rural area of the Yangtze River Delta region during harvest season. *Atmos. Chem. Phys.* **2015**, *15*, 6101–6111. [[CrossRef](#)]
28. Su, R.; Lu, K.; Yu, J.; Tan, Z.; Jiang, M.; Li, J.; Xie, S.; Wu, Y.; Zeng, L.; Zhai, C.; et al. Exploration of the formation mechanism and source attribution of ambient ozone in Chongqing with an observation-based model. *Sci. China Earth Sci.* **2018**, *61*, 23–32. [[CrossRef](#)]
29. Ran, L.; Zhao, C.S.; Xu, W.Y.; Han, M.; Lu, X.Q.; Han, S.Q.; Lin, W.L.; Xu, X.B.; Gao, W.; Yu, Q.; et al. Ozone production in summer in the megacities of Tianjin and Shanghai, China: A comparative study. *Atmos. Chem. Phys.* **2012**, *12*, 7531–7542. [[CrossRef](#)]
30. Tan, Z.F.; Lu, K.D.; Jiang, M.Q.; Su, R.; Wang, H.L.; Lou, S.R.; Fu, Q.Y.; Zhai, C.Z.; Tan, Q.W.; Yue, D.L.; et al. Daytime atmospheric oxidation capacity in four Chinese megacities during the photochemically polluted season: A case study based on box model simulation. *Atmos. Chem. Phys.* **2019**, *19*, 3493–3513. [[CrossRef](#)]
31. Xue, L.K.; Wang, T.; Gao, J.; Ding, A.J.; Zhou, X.H.; Blake, D.R.; Wang, X.F.; Saunders, S.M.; Fan, S.J.; Zuo, H.C.; et al. Ground-level ozone in four Chinese cities: Precursors, regional transport and heterogeneous processes. *Atmos. Chem. Phys.* **2014**, *14*, 13175–13188. [[CrossRef](#)]
32. Li, K.; Chen, L.H.; Ying, F.; White, S.J.; Jang, C.; Wu, X.C.; Gao, X.; Hong, S.M.; Shen, J.D.; Azzi, M.; et al. Meteorological and chemical impacts on ozone formation: A case study in Hangzhou, China. *Atmos. Res.* **2017**, *196*, 40–52. [[CrossRef](#)]
33. Lin, H.T.; Wang, M.; Duan, Y.S.; Fu, Q.Y.; Ji, W.H.; Cui, H.X.; Jin, D.; Lin, Y.F.; Hu, K. O₃ sensitivity and contributions of different NMHC sources in O₃ formation at urban and suburban sites in Shanghai. *Atmosphere* **2020**, *11*, 295. [[CrossRef](#)]
34. Zhao, Y.; Chen, L.; Li, K.; Han, L.; Zhang, X.; Wu, X.; Gao, X.; Azzi, M.; Cen, K. Atmospheric ozone chemistry and control strategies in Hangzhou, China: Application of a 0-D box model. *Atmos. Res.* **2020**, *246*, 105109. [[CrossRef](#)]
35. Ling, Z.H.; Guo, H. Contribution of VOC sources to photochemical ozone formation and its control policy implication in Hong Kong. *Environ. Sci. Policy* **2014**, *38*, 180–191. [[CrossRef](#)]
36. He, Z.R.; Wang, X.M.; Ling, Z.H.; Zhao, J.; Guo, H.; Shao, M.; Wang, Z. Contributions of different anthropogenic volatile organic compound sources to ozone formation at a receptor site in the Pearl River Delta region and its policy implications. *Atmos. Chem. Phys.* **2019**, *19*, 8801–8816. [[CrossRef](#)]
37. Yu, D.; Tan, Z.F.; Lu, K.D.; Ma, X.F.; Li, X.; Chen, S.Y.; Zhu, B.; Lin, L.L.; Li, Y.T.; Qiu, P.P.; et al. An explicit study of local ozone budget and NO_x-VOCs sensitivity in Shenzhen China. *Atmos. Environ.* **2020**, *224*, 117304. [[CrossRef](#)]
38. Shen, H.Q.; Liu, Y.H.; Zhao, M.; Li, J.; Zhang, Y.N.; Yang, J.; Jiang, Y.; Chen, T.S.; Chen, M.; Huang, X.B.; et al. Significance of carbonyl compounds to photochemical ozone formation in a coastal city (Shantou) in eastern China. *Sci. Total Environ.* **2021**, *764*, 144031. [[CrossRef](#)]
39. Zou, Y.; Deng, X.J.; Deng, T.; Yin, C.Q.; Li, F. One-year characterization and reactivity of isoprene and its impact on surface ozone formation at a suburban site in Guangzhou, China. *Atmosphere* **2019**, *10*, 201. [[CrossRef](#)]
40. Liu, X.; Wang, N.; Lyu, X.; Zeren, Y.; Jiang, F.; Wang, X.; Zou, S.; Ling, Z.; Guo, H. Photochemistry of ozone pollution in autumn in Pearl River Estuary, South China. *Sci. Total Environ.* **2021**, *754*, 141812. [[CrossRef](#)]
41. Wang, J.; Zhang, Y.L.; Wu, Z.F.; Luo, S.L.; Song, W.; Wang, X.M. Ozone episodes during and after the 2018 Chinese National Day holidays in Guangzhou: Implications for the control of precursor VOCs. *J. Environ. Sci.* **2022**, *114*, 322–333. [[CrossRef](#)] [[PubMed](#)]
42. Lei, X.W.; Cheng, H.R.; Peng, J.; Jiang, H.M.; Lyu, X.P.; Zeng, P.; Wang, Z.W.; Guo, H. Impact of long-range atmospheric transport on volatile organic compounds and ozone photochemistry at a regional background site in central China. *Atmos. Environ.* **2021**, *246*, 118093. [[CrossRef](#)]
43. Xie, Y.T.; Cheng, C.L.; Wang, Z.H.; Wang, K.; Wang, Y.; Zhang, X.C.; Li, X.H.; Ren, L.J.; Liu, M.; Li, M. Exploration of O₃-precursor relationship and observation-oriented O₃ control strategies in a non-provincial capital city, southwestern China. *Sci. Total Environ.* **2021**, *800*, 149422. [[CrossRef](#)] [[PubMed](#)]
44. Chameides, W.L.; Lindsay, R.W.; Richardson, J.; Kiang, C.S. The role of biogenic hydrocarbons in urban photochemical smog: Atlanta as a case study. *Science* **1988**, *241*, 1473–1475. [[CrossRef](#)]
45. Ryerson, T.B.; Trainer, M.; Holloway, J.S.; Parrish, D.D.; Huey, L.G.; Sueper, D.T.; Frost, G.J.; Donnelly, S.G.; Schauffler, S.; Atlas, E.L.; et al. Observations of ozone formation in power plant plumes and implications for ozone control strategies. *Science* **2001**, *292*, 719–723. [[CrossRef](#)]
46. Chen, W.H.; Guenther, A.B.; Wang, X.M.; Chen, Y.H.; Gu, D.S.; Chang, M.; Zhou, S.Z.; Wu, L.L.; Zhang, Y.Q. Regional to global biogenic isoprene emission responses to changes in vegetation from 2000 to 2015. *J. Geophys. Res. Atmos.* **2018**, *123*, 3757–3771. [[CrossRef](#)]
47. Tie, X.X.; Li, G.H.; Ying, Z.M.; Guenther, A.; Madronich, S. Biogenic emissions of isoprenoids and NO in China and comparison to anthropogenic emissions. *Sci. Total Environ.* **2006**, *371*, 238–251. [[CrossRef](#)]
48. Chan, C.K.; Yao, X. Air pollution in mega cities in China. *Atmos. Environ.* **2008**, *42*, 1–42. [[CrossRef](#)]

49. Zou, Y.; Deng, X.J.; Zhu, D.; Gong, D.C.; Wang, H.; Li, F.; Tan, H.B.; Deng, T.; Mai, B.R.; Liu, X.T.; et al. Characteristics of 1 year of observational data of VOCs, NO_x and O₃ at a suburban site in Guangzhou, China. *Atmos. Chem. Phys.* **2015**, *15*, 6625–6636. [[CrossRef](#)]
50. Guenther, A.; Zimmerman, P.; Wildermuth, M. Natural volatile organic compound emission rate emissions for U.S. woodland landscapes. *Atmos. Environ.* **1994**, *28*, 1197–1210. [[CrossRef](#)]
51. Klinger, L.F.; Li, Q.J.; Guenther, A.B.; Greenberg, J.P.; Baker, B.; Bai, J.H. Assessment of volatile organic compound emissions from ecosystems of China. *J. Geophys. Res. Atmos.* **2002**, *107*, 4603. [[CrossRef](#)]
52. Leung, D.Y.C.; Wong, P.; Cheung, B.K.H.; Guenther, A. Improved land cover and emission factors for modeling biogenic volatile organic compounds emissions from Hong Kong. *Atmos. Environ.* **2010**, *44*, 1456–1468. [[CrossRef](#)]
53. Zheng, J.; Zheng, Z.; Yu, Y.; Zhong, L. Temporal, spatial characteristics and uncertainty of biogenic VOC emissions in the Pearl River Delta region, China. *Atmos. Environ.* **2010**, *44*, 1960–1969. [[CrossRef](#)]
54. Wang, X.M.; Situ, S.P.; Guenther, A.; Chen, F.; Wu, Z.Y.; Xia, B.C.; Wang, T.J. Spatiotemporal variability of biogenic terpenoid emissions in Pearl River Delta, China, with high-resolution land-cover and meteorological data. *Tellus Ser. B-Chem. Phys. Meteorol.* **2011**, *63*, 241–254. [[CrossRef](#)]
55. Situ, S.; Guenther, A.; Wang, X.; Jiang, X.; Turnipseed, A.; Wu, Z.; Bai, J.; Wang, X. Impacts of seasonal and regional variability in biogenic VOC emissions on surface ozone in the Pearl River delta region, China. *Atmos. Chem. Phys.* **2013**, *13*, 11803–11817. [[CrossRef](#)]
56. Wu, K.; Yang, X.Y.; Chen, D.; Gu, S.; Lu, Y.Q.; Jiang, Q.; Wang, K.; Ou, Y.H.; Qian, Y.; Shao, P.; et al. Estimation of biogenic VOC emissions and their corresponding impact on ozone and secondary organic aerosol formation in China. *Atmos. Res.* **2020**, *231*, 104656. [[CrossRef](#)]
57. Wang, H.L.; Wu, K.; Liu, Y.M.; Sheng, B.S.; Lu, X.; He, Y.P.; Xie, J.L.; Wang, H.C.; Fan, S.J. Role of heat wave-induced biogenic VOC enhancements in persistent ozone episodes formation in Pearl River Delta. *J. Geophys. Res. Atmos.* **2021**, *126*, e2020JD034317. [[CrossRef](#)]
58. Li, L.Y.; Chen, Y.; Xie, S.D. Spatio-temporal variation of biogenic volatile organic compounds emissions in China. *Environ. Pollut.* **2013**, *182*, 157–168. [[CrossRef](#)]
59. Zeng, J.Q.; Song, W.; Zhang, Y.L.; Mu, Z.B.; Pang, W.H.; Zhang, H.N.; Wang, X.M. Emissions of isoprenoids from dominant tree species in subtropical China. *Front. For. Glob. Chang.* **2022**, *5*, 1089676. [[CrossRef](#)]
60. Zhang, Y.L.; Wang, X.M.; Blake, D.R.; Li, L.F.; Zhang, Z.; Wang, S.Y.; Guo, H.; Lee, F.S.C.; Gao, B.; Chan, L.Y.; et al. Aromatic hydrocarbons as ozone precursors before and after outbreak of the 2008 financial crisis in the Pearl River Delta region, south China. *J. Geophys. Res. Atmos.* **2012**, *117*, D15306. [[CrossRef](#)]
61. Zhang, Y.L.; Wang, X.M.; Barletta, B.; Simpson, I.J.; Blake, D.R.; Fu, X.X.; Zhang, Z.; He, Q.F.; Liu, T.Y.; Zhao, X.Y.; et al. Source attributions of hazardous aromatic hydrocarbons in urban, suburban and rural areas in the Pearl River Delta (PRD) region. *J. Hazard. Mater.* **2013**, *250*, 403–411. [[CrossRef](#)] [[PubMed](#)]
62. Zhang, Y.L.; Wang, X.M.; Zhang, Z.; Lu, S.J.; Huang, Z.H.; Li, L.F. Sources of C₂–C₄ alkenes, the most important ozone nonmethane hydrocarbon precursors in the Pearl River Delta region. *Sci. Total Environ.* **2015**, *502*, 236–245. [[CrossRef](#)]
63. Yang, W.; Zhang, Y.; Wang, X.; Li, S.; Zhu, M.; Yu, Q.; Li, G.; Huang, Z.; Zhang, H.; Wu, Z.; et al. Volatile organic compounds at a rural site in Beijing: Influence of temporary emission control and wintertime heating. *Atmos. Chem. Phys.* **2018**, *18*, 12663–12682. [[CrossRef](#)]
64. Wu, Z.F.; Zhang, Y.L.; He, J.J.; Chen, H.Z.; Huang, X.L.; Wang, Y.J.; Yu, X.; Yang, W.Q.; Zhang, R.Q.; Zhu, M.; et al. Dramatic increase in reactive volatile organic compound (VOC) emissions from ships at berth after implementing the fuel switch policy in the Pearl River Delta Emission Control Area. *Atmos. Chem. Phys.* **2020**, *20*, 1887–1900. [[CrossRef](#)]
65. Wu, Z.F.; Zhang, Y.L.; Pei, C.L.; Huang, Z.Z.; Wang, Y.J.; Chen, Y.N.; Yan, J.H.; Huang, X.Q.; Xiao, S.X.; Luo, S.L.; et al. Real-world emissions of carbonyls from vehicles in an urban tunnel in south China. *Atmos. Environ.* **2021**, *258*, 118491. [[CrossRef](#)]
66. Jenkin, M.E.; Saunders, S.M.; Wagner, V.; Pilling, M.J. Protocol for the development of the Master Chemical Mechanism, MCM v3 (Part B): Tropospheric degradation of aromatic volatile organic compounds. *Atmos. Chem. Phys.* **2003**, *3*, 181–193. [[CrossRef](#)]
67. Jenkin, M.E.; Young, J.C.; Rickard, A.R. The MCM v3.3.1 degradation scheme for isoprene. *Atmos. Chem. Phys.* **2015**, *15*, 11433–11459. [[CrossRef](#)]
68. Saunders, S.M.; Jenkin, M.E.; Derwent, R.G.; Pilling, M.J. Protocol for the development of the Master Chemical Mechanism, MCM v3 (Part A): Tropospheric degradation of non-aromatic volatile organic compounds. *Atmos. Chem. Phys.* **2003**, *3*, 161–180. [[CrossRef](#)]
69. Sommariva, R.; Cox, S.; Martin, C.; Boronska, K.; Young, J.; Jimack, P.K.; Pilling, M.J.; Matthaios, V.N.; Nelson, B.S.; Newland, M.J.; et al. AtChem (version 1), an open-source box model for the Master Chemical Mechanism. *Geosci. Model Dev.* **2020**, *13*, 169–183. [[CrossRef](#)]
70. Huang, J.P.; Fung, J.C.H.; Lau, A.K.H.; Qin, Y. Numerical simulation and process analysis of typhoon-related ozone episodes in Hong Kong. *J. Geophys. Res. Atmos.* **2005**, *110*, D05301. [[CrossRef](#)]
71. Cardelino, C.A.; Chameides, W.L. An observation-based model for analyzing ozone precursor relationships in the urban atmosphere. *J. Air Waste Manag. Assoc.* **1995**, *45*, 161–180. [[CrossRef](#)] [[PubMed](#)]

72. Lyu, X.P.; Guo, H.; Simpson, I.J.; Meinardi, S.; Louie, P.K.K.; Ling, Z.H.; Wang, Y.; Liu, M.; Luk, C.W.Y.; Wang, N.; et al. Effectiveness of replacing catalytic converters in LPG-fueled vehicles in Hong Kong. *Atmos. Chem. Phys.* **2016**, *16*, 6609–6626. [[CrossRef](#)]
73. Huang, W.; Zhao, Q.; Liu, Q.; Chen, F.; He, Z.; Guo, H.; Ling, Z. Assessment of atmospheric photochemical reactivity in the Yangtze River Delta using a photochemical box model. *Atmos. Res.* **2020**, *245*, 105088. [[CrossRef](#)]
74. Hui, L.R.; Liu, X.G.; Tan, Q.W.; Feng, M.; An, J.L.; Qu, Y.; Zhang, Y.H.; Jiang, M.Q. Characteristics, source apportionment and contribution of VOCs to ozone formation in Wuhan, Central China. *Atmos. Environ.* **2018**, *192*, 55–71. [[CrossRef](#)]
75. Lu, X.; Zhang, L.; Chen, Y.F.; Zhou, M.; Zheng, B.; Li, K.; Liu, Y.M.; Lin, J.T.; Fu, T.M.; Zhang, Q. Exploring 2016–2017 surface ozone pollution over China: Source contributions and meteorological influences. *Atmos. Chem. Phys.* **2019**, *19*, 8339–8361. [[CrossRef](#)]
76. Ren, J.; Hao, Y.F.; Simayi, M.; Shi, Y.Q.; Xie, S.D. Spatiotemporal variation of surface ozone and its causes in Beijing, China since 2014. *Atmos. Environ.* **2021**, *260*, 118556. [[CrossRef](#)]
77. Deng, C.; Tian, S.; Li, Z.; Li, K. Spatiotemporal characteristics of PM_{2.5} and ozone concentrations in Chinese urban clusters. *Chemosphere* **2022**, *295*, 133813. [[CrossRef](#)]
78. Yang, Y.D.; Shao, M.; Kessel, S.; Li, Y.; Lu, K.D.; Lu, S.H.; Williams, J.; Zhang, Y.H.; Zeng, L.M.; Noelscher, A.C.; et al. How the OH reactivity affects the ozone production efficiency: Case studies in Beijing and Heshan, China. *Atmos. Chem. Phys.* **2017**, *17*, 7127–7142. [[CrossRef](#)]
79. Zhu, J.; Wang, S.; Wang, H.; Jing, S.; Lou, S.; Saiz-Lopez, A.; Zhou, B. Observationally constrained modeling of atmospheric oxidation capacity and photochemical reactivity in Shanghai, China. *Atmos. Chem. Phys.* **2020**, *20*, 1217–1232. [[CrossRef](#)]
80. Yang, Y.C.; Liu, X.G.; Zheng, J.; Tan, Q.W.; Feng, M.; Qu, Y.; An, J.L.; Cheng, N.L. Characteristics of one-year observation of VOCs, NO_x, and O₃ at an urban site in Wuhan, China. *J. Environ. Sci.* **2019**, *79*, 297–310. [[CrossRef](#)]
81. Pei, C.L.; Yang, W.Q.; Zhang, Y.L.; Song, W.; Xiao, S.X.; Wang, J.; Zhang, J.P.; Zhang, T.; Chen, D.H.; Wang, Y.J.; et al. Decrease in ambient volatile organic compounds during the COVID-19 lockdown period in the Pearl River Delta region, south China. *Sci. Total Environ.* **2022**, *823*, 153720. [[CrossRef](#)] [[PubMed](#)]
82. Liu, X.; Lyu, X.; Wang, Y.; Jiang, F.; Guo, H. Intercomparison of O₃ formation and radical chemistry in the past decade at a suburban site in Hong Kong. *Atmos. Chem. Phys.* **2019**, *19*, 5127–5145. [[CrossRef](#)]
83. Meng, Y.; Song, J.; Zeng, L.; Zhang, Y.; Zhao, Y.; Liu, X.; Guo, H.; Zhong, L.; Ou, Y.; Zhou, Y.; et al. Ambient volatile organic compounds at a receptor site in the Pearl River Delta region: Variations, source apportionment and effects on ozone formation. *J. Environ. Sci.* **2022**, *111*, 104–117. [[CrossRef](#)] [[PubMed](#)]
84. Barletta, B.; Meinardi, S.; Simpson, I.J.; Zou, S.; Rowland, F.S.; Blake, D.R. Ambient mixing ratios of nonmethane hydrocarbons (NMHCs) in two major urban centers of the Pearl River Delta (PRD) region: Guangzhou and Dongguan. *Atmos. Environ.* **2008**, *42*, 4393–4408. [[CrossRef](#)]
85. Tang, J.H.; Chu, K.W.; Chan, L.Y.; Chen, Y.J. Non-methane hydrocarbon emission profiles from printing and electronic industrial processes and its implications on the ambient atmosphere in the Pearl River Delta, South China. *Atmos. Pollut. Res.* **2014**, *5*, 151–160. [[CrossRef](#)]
86. Han, D.M.; Wang, Z.; Cheng, J.P.; Wang, Q.; Chen, X.J.; Wang, H.L. Volatile organic compounds (VOCs) during non-haze and haze days in Shanghai: Characterization and secondary organic aerosol (SOA) formation. *Environ. Sci. Pollut. Res.* **2017**, *24*, 18619–18629. [[CrossRef](#)]
87. Guo, H.; Jiang, F.; Cheng, H.R.; Simpson, I.J.; Wang, X.M.; Ding, A.J.; Wang, T.J.; Saunders, S.M.; Wang, T.; Lam, S.H.M.; et al. Concurrent observations of air pollutants at two sites in the Pearl River Delta and the implication of regional transport. *Atmos. Chem. Phys.* **2009**, *9*, 7343–7360. [[CrossRef](#)]
88. Chou, C.C.K.; Tsai, C.Y.; Chang, C.C.; Lin, P.H.; Liu, S.C.; Zhu, T. Photochemical production of ozone in Beijing during the 2008 Olympic Games. *Atmos. Chem. Phys.* **2011**, *11*, 9825–9837. [[CrossRef](#)]
89. Zong, R.H.; Yang, X.; Wen, L.; Xu, C.H.; Zhu, Y.H.; Chen, T.S.; Yao, L.; Wang, L.W.; Zhang, J.M.; Yang, L.X.; et al. Strong ozone production at a rural site in the North China Plain: Mixed effects of urban plumes and biogenic emissions. *J. Environ. Sci.* **2018**, *71*, 261–270. [[CrossRef](#)]
90. Fu, T.M.; Zheng, Y.Q.; Paulot, F.; Mao, J.Q.; Yantosca, R.M. Positive but variable sensitivity of August surface ozone to large-scale warming in the southeast United States. *Nat. Clim. Chang.* **2015**, *5*, 454–458. [[CrossRef](#)]
91. Guidolotti, G.; Palozzi, E.; Gavrichkova, O.; Scartazza, A.; Mattioni, M.; Loreto, F.; Calfapietra, C. Emission of constitutive isoprene, induced monoterpenes, and other volatiles under high temperatures in *Eucalyptus camaldulensis*: A C-13 labelling study. *Plant Cell Environ.* **2019**, *42*, 1929–1938. [[CrossRef](#)] [[PubMed](#)]
92. Yanez-Serrano, A.M.; Bourtsoukidis, E.; Alves, E.G.; Bauwens, M.; Stavrakou, T.; Llusia, J.; Filella, I.; Guenther, A.; Williams, J.; Artaxo, P.; et al. Amazonian biogenic volatile organic compounds under global change. *Glob. Chang. Biol.* **2020**, *26*, 4722–4751. [[CrossRef](#)] [[PubMed](#)]
93. Cheng, H.R.; Guo, H.; Wang, X.M.; Saunders, S.M.; Lam, S.H.M.; Jiang, F.; Wang, T.J.; Ding, A.J.; Lee, S.C.; Ho, K.F. On the relationship between ozone and its precursors in the Pearl River Delta: Application of an observation-based model (OBM). *Environ. Sci. Pollut. Res.* **2010**, *17*, 547–560. [[CrossRef](#)] [[PubMed](#)]
94. Wang, Y.; Wang, H.; Guo, H.; Lyu, X.P.; Cheng, H.R.; Ling, Z.H.; Louie, P.K.K.; Simpson, I.J.; Meinardi, S.; Blake, D.R. Long-term O₃-precursor relationships in Hong Kong: Field observation and model simulation. *Atmos. Chem. Phys.* **2017**, *17*, 10919–10935. [[CrossRef](#)]

95. Zhu, J.X.; Cheng, H.R.; Peng, J.; Zeng, P.; Wang, Z.W.; Lyu, X.P.; Guo, H. O₃ photochemistry on O₃ episode days and non-O₃ episode days in Wuhan, Central China. *Atmos. Environ.* **2020**, *223*, 117236. [[CrossRef](#)]
96. Zhang, T.; Xiao, S.X.; Wang, X.M.; Zhang, Y.L.; Pei, C.L.; Chen, D.H.; Jiang, M.; Liao, T. Volatile organic compounds monitored online at three photochemical assessment monitoring stations in the Pearl River Delta (PRD) region during summer 2016: Sources and emission areas. *Atmosphere* **2021**, *12*, 327. [[CrossRef](#)]
97. Zheng, J.Y.; Yu, Y.F.; Mo, Z.W.; Zhang, Z.; Wang, X.M.; Yin, S.S.; Peng, K.; Yang, Y.; Feng, X.Q.; Cai, H.H. Industrial sector-based volatile organic compound (VOC) source profiles measured in manufacturing facilities in the Pearl River Delta, China. *Sci. Total Environ.* **2013**, *456*, 127–136. [[CrossRef](#)] [[PubMed](#)]
98. McDonald, B.C.; Goldstein, A.H.; Harley, R.A. Long-term trends in California mobile source emissions and ambient concentrations of black carbon and organic aerosol. *Environ. Sci. Technol.* **2015**, *49*, 5178–5188. [[CrossRef](#)]
99. Mo, Z.W.; Shao, M.; Lu, S.H. Compilation of a source profile database for hydrocarbon and OVOC emissions in China. *Atmos. Environ.* **2016**, *143*, 209–217. [[CrossRef](#)]
100. Sha, Q.E.; Zhu, M.N.; Huang, H.W.; Wang, Y.Z.; Huang, Z.J.; Zhang, X.C.; Tang, M.S.; Lu, M.H.; Chen, C.; Shi, B.W.; et al. A newly integrated dataset of volatile organic compounds (VOCs) source profiles and implications for the future development of VOCs profiles in China. *Sci. Total Environ.* **2021**, *793*, 148348. [[CrossRef](#)]

Disclaimer/Publisher’s Note: The statements, opinions and data contained in all publications are solely those of the individual author(s) and contributor(s) and not of MDPI and/or the editor(s). MDPI and/or the editor(s) disclaim responsibility for any injury to people or property resulting from any ideas, methods, instructions or products referred to in the content.